THE ROYAL SOCIETY

Received 16 October 2001
Accepted 11 January 2002
Published online 25 March 2002

Visualizing patterns of craniofacial shape variation in *Homo sapiens*

Christoph P. E. Zollikofer* **and Marcia S. Ponce de León**

Anthropologisches Institut and Institut für Informatik, MultiMedia Laboratorium, Universität Zürich-Irchel, Winterthurerstrasse 190, CH-8057 Zürich, Switzerland

The geometric morphometric analysis of shape variation in complex biological structures such as the human skull poses a number of specific challenges: the registration of homologous morphologies, the treatment of bilateral symmetry, the graphical representation of form variability in three dimensions and the interpretation of the results in terms of differential growth processes. To visualize complex patterns of shape change, we propose an alternative to classical Cartesian deformation grids in the style of D'Arcy W. Thompson. Reference to the surface structures of the organism under investigation permits a comprehensive visual grasp of shape change and its tentative interpretation in terms of differential growth. The application of this method to the analysis of human craniofacial shape variation reveals distinct modes of growth and development of the neurocranial and viscerocranial regions of the skull. Our data further indicate that variations in the orientation of the viscerocranium relative to the neurocranium impinge on the shapes of the face and the cranial vault.

Keywords: allometry; cranial development; geometric morphometrics; growth; *Homo sapiens*; symmetry

1. INTRODUCTION

The recent advent of geometric morphometric methods (GMM) has considerably modified the ways in which variation of organismic form is measured and treated statistically (Rohlf & Marcus 1993). GMM aim at integration of the real-space geometric properties of biological structures into multivariate analyses by means of anatomical points of reference—so-called landmarks—which are explicitly chosen to represent locations of biological and geometric homology. The mathematical equivalent of the biological homology relationship can be established with Thin Plate Spline (TPS) functions—which act as spatially pervasive mapping functions between landmark configurations (Bookstein 1991)—or through the exhaustive analysis of all between-landmark distances in a configuration (Euclidean Distance Matrix Analysis; Lele 1993; Richtsmeier & Lele 1993). GMM are especially well-suited to study cranial morphology, as the skull is an essentially rigid structure, whose complex surface displays numerous well-defined landmarks representing locations of homology. Accordingly, GMM have already been used extensively for the analysis of variation in craniofacial shape and its covariation with external variables such as taxon, sex, size, age, and environmental and pathological factors (Zelditch *et al.* 1992; Loy *et al.* 1993; Richtsmeier & Walker 1993; Richtsmeier *et al.* 1993; Lynch *et al.* 1996; Yaroch 1996; O'Higgins & Jones 1998; Rao & Suryawanshi 1998; Adams & Rohlf 2000; O'Higgins 2000).

Making explicit reference to skulls as bilaterally organized three-dimensional (3D) structures poses three specific problems.

(i) Bilateral symmetry. On the one hand, bilateral structures represent a special case of within-specimen covariation of shape. Natural deviations from symmetry in the form of fluctuating or directional asymmetry represent patterns of covariation on their own, the statistical treatment of which needs special consideration (Emlen *et al.* 1993; Auffray *et al.* 1996; Klingenberg *et al.* 1998; Klingenberg & Nijhout 1999; Mardia *et al.* 2000). On the other hand, in an analysis focusing on patterns of bilateral shape variation (rather than deviations from symmetry), it is necessary to devise methods which render specimens symmetrical relative to their midplane. This would constrain modes of shape variation resulting from statistical shape analysis (Dryden & Mardia 1998) not to bend the midplane of the structures under investigation.

(ii) Homology of landmarks. In GMM, the definition of landmarks—and thus the definition of homology relationships between specimens—depends on the type of questions asked. For example, on the one hand, in the present growth-orientated study of cranial variation, landmarks are used that denote centres of bone growth, or boundaries between cranial subregions. On the other hand, a comparative biomechanical analysis may lay more emphasis on landmarks characterizing the geometry of lever arms. It is further readily recognizable that the distribution of suitable landmarks over the skull is highly inhomogeneous. For example, the maxillofacial region is rich in well-defined landmarks, whereas the cranial vault exhibits relatively few landmarks. Various methods have therefore been proposed to sample morphologies more evenly and extensively (Cutting *et al.* 1993, 1995; Bookstein 1997; Bookstein *et al.* 1999; Andresen *et al.* 2000; Andresen & Nielsen 2001). While such surface-bounded methods permit dense sampling, an unresolved problem arises from the fact that the resulting 'semi-landmarks' (Bookstein 1997) represent locations of

* Author for correspondence (zolli@ifi.unizh.ch).

© 2002 The Royal Society

primarily geometric homology, in which biological homology relationships are only partially preserved. It is therefore necessary to find a compromise between geometry-driven dense sampling and explicit representation of biological homology.

(iii) Rendering patterns of 3D shape variation. During the visualization of patterns of shape variability in 3D, the use of deformation grids (Thompson 1948) in a biological context is limited for several reasons. The first is a practical one. While grids represent a suitable means to visualize shape change in two dimensions (2D), substantial problems arise in 3D: 3D cuboid grids or 2D square grids positioned in space tend to be unintelligible, because our visual attention is directed towards undesired boundary effects at the edges of the grid—which no longer have any relationship with the biological structure itself—while more significant internal alterations remain unnoticed (Dryden & Mardia 1998; O'Higgins & Jones 1998). The second reason is fundamental: deformation grids introduce an external system of geometric reference which is not directly related to the original organismic geometry. This makes it difficult to interpret geometric 'deformation' in terms of potential biological mechanisms of shape variation.

In this paper, these issues are addressed with the specific aim of quantifying and visualizing shape variation in the growing human skull. Building upon arguments proposed by Mardia *et al.* (2000), we present a method which permits analysis of bilaterally symmetrical shape variation independent of patterns of deviation from symmetry. Furthermore, during visualization of shape variation, a method is proposed which makes explicit reference to the intrinsic geometry of the biological structures under examination. We show that the combination of these techniques facilitates the interpretation of patterns of cranial shape variation in *Homo sapiens* in terms of morphogenetic mechanisms. Evolutionary developmental aspects of hominid cranial shape variability have recently received specific attention (McCollum 1999; Lieberman *et al.* 2000*a*,*b*; Ponce de León & Zollikofer 2001), notably with respect to their role as a potential source of morphological novelty during human phylogeny. The patterns of shape variation in *H. sapiens* skulls analysed here may serve as a model to illustrate how developmental variability may have given rise to pervasive modifications of craniofacial morphologies in the course of hominid evolution.

2. METHODS

(a) *Sample*

The sample consisted of 12 immature and 8 adult craniomandibular skeletal specimens of *H. sapiens* ($n = 20$). We used a pooled-population/pooled-sex sample of modern ($n_m = 18$) and fossil specimens ($n_f = 2$; specimens 9 and 11 from the site of Qafzeh, Israel) to represent morphological variability in developmental stage (from the age of 3 years to adulthood), size, geographical range and geological time. Individual ages were estimated using standard dental eruption scores (Ubelaker 1978). Volume data of all specimens were acquired with computer tomography. 3D-surface representations derived from these data were used to determine the locations of 17 midsagittal cranio-mandibular landmarks and 23 pairs of bilateral landmarks ($p = 63$). The landmarks were chosen to represent locations of between-specimen homology in the growing cranium (such as meeting points between three or more cranial bones and/or the midsagittal plane, centres of cranial foramina, and centres of growth of the frontal and parietal bones). As the cranial vault exhibits relatively few landmarks, additional points of reference were defined at midpoints along interosseous sutures (see electronic Appendix A, available on The Royal Society's Publications Web site, for sample details and landmark definitions).

(b) *Analysis of symmetrical shape variability*

The form of each specimen i, as defined by its landmark configuration X_i (a $3 \times p$ matrix of the 3D coordinates of the p landmarks), has two basic constituents, 'size' and 'shape', which characterize the extent and the geometry of the configuration, respectively. Size is given by centroid size S (the square root of the sum of squared distances of each landmark from the centre of mass of the X_i; Bookstein (1991)). Prior to the evaluation of a sample consensus configuration, each specimen is made symmetrical through generalized least-squares (GLS) superposition (Rohlf & Slice 1990) of X_i with its own reflection X_i', such that the resulting average specimen $\bar{X}_i$ is precisely symmetrical with respect to its own least-squares midplane. Subsequently, specimens $\bar{X}_i$ are size-normalized and GLS-superimposed to evaluate a symmetrical consensus $\bar{C}$. An alternative method of symmetrization consists in evaluating $\bar{C}$ by GLS superposition of all specimens X and their reflections X' together (Mardia *et al.* 2000), followed by specimen-wise averaging of X_i and X_i'. We will refer to these methods as self- and sample-symmetrization, respectively.

In both cases, the specimens' coordinates in linearized Procrustes space are given by

$$\bar{V}_i = \bar{X}_i - \bar{C}. \tag{2.1}$$

V_i is a $3 \times p$ matrix denoting the linear deviation (landmark coordinate by landmark coordinate) of specimen X_i from the consensus C.

Shape variability in the sample is studied with principal components (PC) analysis (Dryden & Mardia 1998)

$$M_{\mathrm{cov}} = \bar{V} \cdot \bar{V}^T = E \Lambda E^T, \tag{2.2}$$

where M_{cov} is the within-sample covariance matrix, E is the matrix of orthogonal eigenvectors and Λ the corresponding diagonal matrix of the eigenvalues of E. ^{T} denotes the matrix transpose. Typically, the first few PCs contain a significant proportion of the total sample variance, such that the dimensionality of the dataset can be reduced considerably. Accordingly, plotting the specimens' PC scores E'

$$E' = E\Lambda, \tag{2.3}$$

for the PCs associated with the largest eigenvalues typically suffices to reveal the biologically meaningful variation in shape.

(c) *Visualization of patterns of shape variation*

An arbitrary point E'_ψ in PC space corresponds to a hypothetical specimen X_ψ in physical space (Dryden & Mardia 1998)

$$X_\psi = C + E'_\psi \cdot E^T. \tag{2.4}$$

It is thus possible to re-express and visualize the results

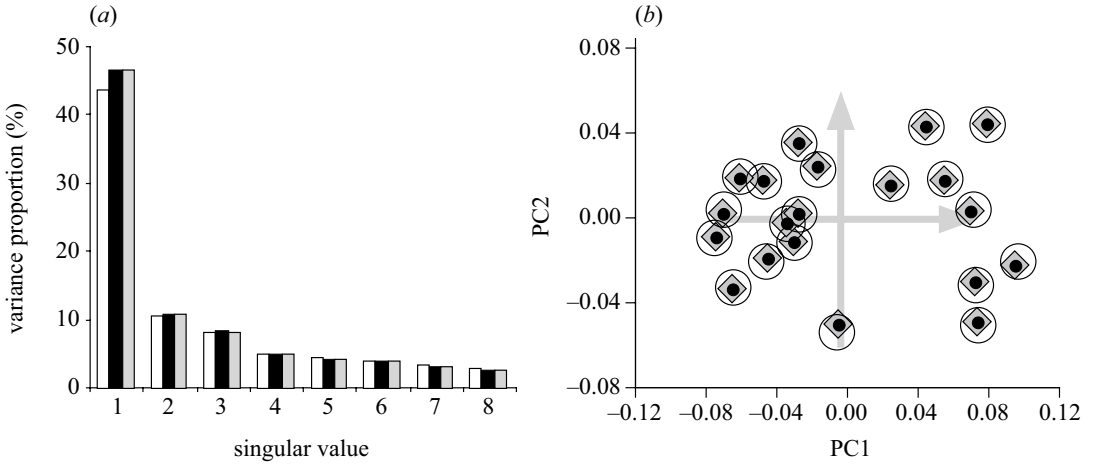

Figure 1. PC analysis of cranio-mandibular shape variation in *Homo sapiens*. Analyses were performed for the original landmark configurations (white), the self-symmetrized (black) and the sample-symmetrized configurations (grey). (*a*) Distribution of the variance proportions for the eight most significant PCs. (*b*) Patterns of distribution of the specimens in PC space exhibit close similarity between analyses. Deviations between the original and the symmetrized shapes hint at left/right asymmetry of specimens. The grey arrows indicate shape transformations along PC1 and PC2, whose geometric implications are illustrated in figure 3.

obtained in PC space in terms of morphology. The transformation of the consensus morphology C into specimen X_ψ can be represented with a TPS interpolation function f_ψ:

$$f_\psi : C \mapsto X_\psi. \tag{2.5}$$

We visualize the effects of f_ψ with explicit reference to the original organismic geometry rather than to a Cartesian deformation grid. Let us recall that the landmarks, which form the basis of the geometric morphometric analysis (and which constitute the nodes of the TPS function f_ψ) are typically derived from surface structures of the specimens. During visualization, it is therefore sensible to make explicit reference to these object surfaces rather than to an arbitrary Cartesian coordinate grid. Accordingly, f_ψ is applied to the physical surface $\{S_C\}$ of the consensus C:

$$f_\psi : \{S_C\} \mapsto \{S_\psi\}. \tag{2.6}$$

In practice, $\{S_C\}$ is obtained through TPS transformation of the surface data from a real specimen X_i (see figure 3). The function f_ψ defines a displacement field over the space R^3, such that every point $\boldsymbol{s}_j \in \{S_C\}$ is transformed into $\boldsymbol{s}_{\psi j} \in \{S_\psi\}$

$$\boldsymbol{s}_{\psi j} = \boldsymbol{s}_j + \boldsymbol{d}_j. \tag{2.7}$$

The displacement vector $\boldsymbol{d}_j$ is now decomposed into its normal and tangential components relative to the orientation of the surface in $\boldsymbol{s}_j$:

$$\boldsymbol{d}_j = \boldsymbol{d}_{j\perp} + \boldsymbol{d}_{j//}. \tag{2.8}$$

To visualize the normal component $\boldsymbol{d}_{j\perp}$, we use

$$d_{j\perp} = \boldsymbol{d}_j \cdot \boldsymbol{n}_j, \tag{2.9}$$

where $\boldsymbol{n}_j$ is the local unit surface normal vector in $\boldsymbol{s}_j$. The scalar product $d_{j\perp}$ indicates the magnitude of $\boldsymbol{d}_{j\perp}$ as well as its direction relative to the surface (through its sign) and is colour-coded using opposite colours. The tangential vector component is visualized as a vector field on the cranial surface (see figure 3).

In addition to the visualization of the directional components of shape transformation, we are also interested in assessing direction-independent local magnitudes of shape change. One aspect that needs special consideration, notably in studies using size as an external covariate of shape, is the allometry of shape change. Adhering to our strategy of using the surface structure as a reference, we consider local allometric changes in the area A_j of a local surface patch as a function of the centroid size S of the object:

$$A_j = a_j \cdot S^{2b_j}, \tag{2.10}$$

where a_j is the scaling factor of the allometric relationship, b_j its exponent ($b_j > 1$ and $b_j < 1$ express positive and negative allometry, respectively; $b_j = 1$ isometry), and the factor 2 in the exponent accounts for the allometric relationship between an area (A_j) and a linear measurement (S).

Because shapes were normalized to unit centroid size $S = 1$ prior to PC analysis, we actually observe the quantity

$$A'_j = A_j / S^2 = a_j \cdot S^{2b_j - 2}. \tag{2.11}$$

To estimate local values b_j, we consider the ratio between the areas before (A'_j) and after ($A'_{\psi j}$) the transformation given by equation (2.6)

$$A'_{\psi j} / A'_j = (S'_\psi / S')^{2(b_j - 1)}, \tag{2.12}$$

where S' and S'_ψ denote the sizes before and after transformation. It follows that

$$b_j = 1 + \frac{1}{2} \frac{\ln(A'_{\psi j} / A'_j)}{\ln(S'_\psi / S')}. \tag{2.13}$$

The exponent b_j can be determined empirically on every location of the surface $\{S\}$ in the following way: the quantities A'_j and $A'_{\psi j}$ are derived by area integration over a small local surface patch $\{A_j\}$ before and after applying the transformation f_ψ, while sizes S' and S'_ψ are estimated from empirical regression functions relating the PC scores of the specimens to centroid size S (see figure 2*b*).

The term $\ln(S'_\psi / S')$ represents a scaling factor that can be omitted if one is exclusively interested in visualizing geometric patterns of relative allometry. Accordingly, we may define

$$b'_j = 2(b_j - 1)\ln(S'_\psi / S') = \ln(A'_{\psi j} / A'_j), \tag{2.14}$$

as the relative local deviation from isometry. For visualization, we may proceed as with quantity $d_{j\perp}$ to discern between positive

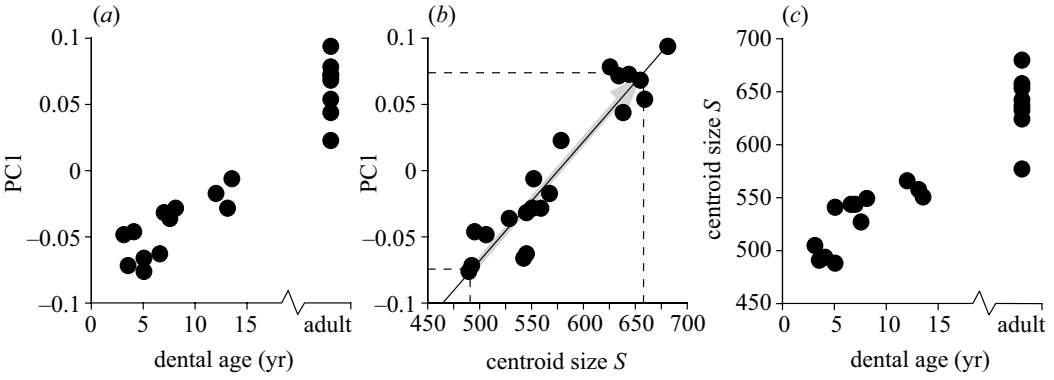

Figure 2. Correlations between PC1 (self-symmetrized shapes; see figure 1*b*), dental age (yr) and centroid size *S*. (*a*) Age-related changes in shape. Note that the variation among adult shapes is similar in magnitude to the variation between the ages of 3 and 15 years. (*b*) The allometric relationship between PC1 and size shows that shape change during growth is closely correlated with changes in size ($r^2 = 0.897$) and that variation among adult shapes is due to differences in size (the size estimates at PC1 $\pm$ 0.075 are used for the evaluation of the allometric exponent *b*; see equation (2.13) and figure 3*b*). (*c*) Age-related changes in size. Note close similarity of this graph with the shape-to-age trajectory (*a*).

and negative values (see figure 3). In geometric terms, b'_j measures the logarithm of the relative contraction or expansion of a local surface patch.

The biological motivation to evaluate these terms is to interpret $d_\perp$, $\boldsymbol{d}_{/\!/}$ and b' as hypothetical relative directions and relative magnitudes of growth. During development of complex 3D structures such as the vertebrate skull, anatomical subregions grow by expansion, drift and/or by passive displacement relative to neighbouring structures (Moss & Young 1960; Enlow 1990). These trends can tentatively be captured by the normal and tangential components of shape change. However, the separate effects of expansion, drift and displacement are not readily distinguishable, as they tend to be superimposed in the observed patterns of translation and rotation of cranial subregions relative to each other. The visualization of local allometric trends represents, therefore, a suitable means to capture the translation- and rotation-invariant aspects of shape change. Altogether, normal/tangential and allometric maps of shape variation (figure 3) combined with direct documentation of growth fields in the human cranium (Enlow 1990) permit interpretation of the observed patterns of shape change in terms of differential mechanisms of growth and development.

3. CRANIAL SHAPE VARIATION IN *HOMO SAPIENS*

We performed PC analysis of shape variation on the original landmark configurations, and on the configurations rendered symmetrical with the two methods described in § 2b, self- and sample-symmetrization (figure 1). As an effect of the elimination of asymmetric shape variation, the symmetrized configurations yield consistently larger variance proportions for each PC than the original configurations (figure 1*a*). Nevertheless, the data scatter in PC space exhibits close similarity between original and symmetrized samples, suggesting that deviations from symmetry do not significantly disturb the basic patterns of symmetrical shape variation in the sample (figure 1*b*). As the two methods of symmetrization yield virtually identical results, we will confine the following considerations to the self-symmetrized dataset.

The PCs represent statistically independent components of shape variability, such that each of them can be tested for correlation with the external variables 'dental age' and 'centroid size (*S*)'. Only the first PC (PC1)—which accounts for 47% of the total shape variability—exhibits correlation with these variables (figure 2). In figure 3*a*,*b*, the morphological implications of shape change during growth are visualized as the transition from a juvenile to an adult specimen (corresponding to the horizontal arrow along PC1 in figure 1*b*). On the one hand, during growth, the mandible and maxilla are expanded in anterior and inferior directions, and the face is elongated. On the other hand, the neurocranium is flattened and undergoes 'relative' contraction. In global terms, a clear separation in quantitative developmental characteristics is revealed between the neurocranium and the viscerocranium, which show negative and positive allometric growth rates, respectively.

In figure 3*c*,*d*, similar procedures were applied to visualize shape variability along the second PC (corresponding to the vertical arrow along PC2 in figure 2*b*). As this component represents shape variation independent of size and age, patterns of shape transformation can no longer be interpreted in terms of growth. However, they indicate positional differences of cranial subregions relative to each other. As evidenced by the lateral cranial views, the neurocranium and viscerocranium tend to 'rotate' in opposite directions relative to each other, resulting in positional rearrangement of the maxillofacial complex relative to the neurocranium. Accordingly, one extreme skull shape (figure 3*c*) is characterized by a high face and a broad, rounded neurocranium, the other extreme (figure 3*d*) by a low midface, a protruding mandible and an elongated, slender neurocranium. The allometric maps show that the transformation between these shapes does not alter the sizes of the braincase and the face relative to each other. Altogether, PC2 captures changes in position and orientation of these cranial subregions relative to each other rather than changes in their relative sizes.

4. CONCLUSIONS

(a) *Patterns of shape variation: biology and geometry*

The fundamental value of GMM resides in their ability to represent the intrinsic geometry of biological structures

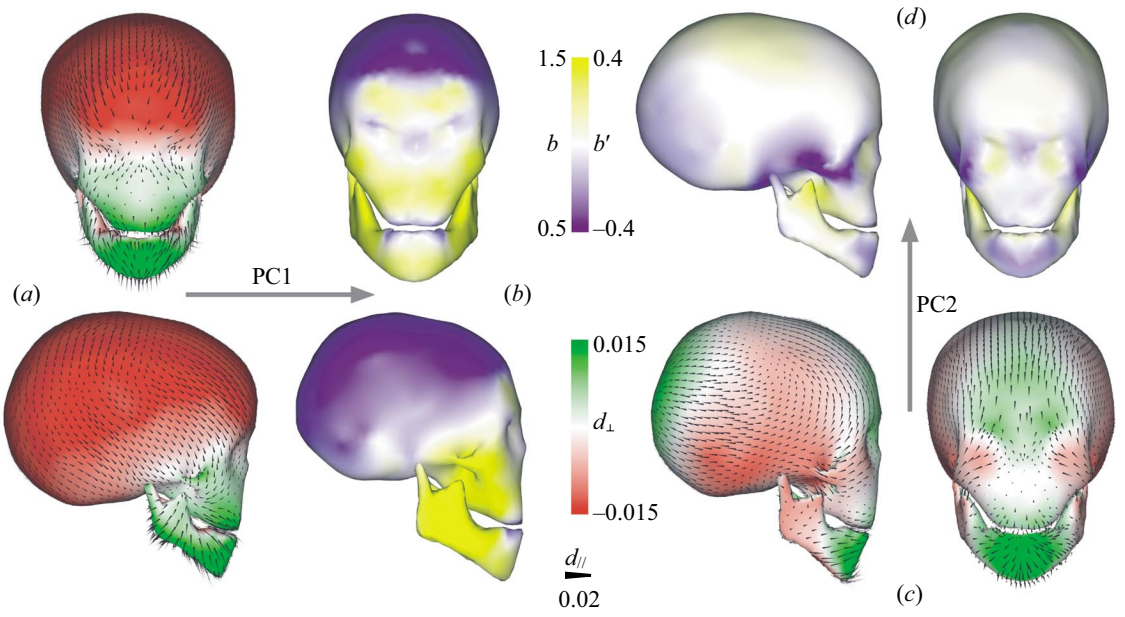

Figure 3. Patterns of cranio-mandibular shape transformation. (*a*,*b*) Shape change from a 3 year old to an adult specimen (corresponding to the horizontal arrow in figure 1*b*). (*a*) The skull shape is shown at the juvenile stage; colours indicate the direction and magnitude of shape change perpendicular to the cranial surface ($\boldsymbol{d}_{\perp}$; green, outward; red, inward; see equation (2.9)); the arrows indicate shape change parallel to the surface ($d_{//}$; see equation (2.8)); all scales in units of centroid size). (*b*) The skull shape is shown at adulthood; colours indicate the relative amount of local growth that was necessary to attain that shape (yellow and blue code for positive and negative allometric growth of the local surface, white indicates isometry; allometric coefficients b and b' were evaluated using equations (2.13) and (2.14), and figure 2*c*). Note the contrasting growth characteristics of the neurocranium and viscerocranium. (*c*,*d*) Size- and age-independent variability in cranial shape (corresponding to the vertical arrow in figure 1*b*). (*c*) and (*d*) show the two extremes of this mode of variation of cranial morphology; in (*c*) shape difference is visualized in directions perpendicular (green and red) and parallel (arrows) to the surface; in (*d*) shape difference is visualized as the amount of surface expansion or contraction (yellow and blue) that results from transformation. Note that this transformation mainly affects the orientation of the braincase and the face relative to each other, while their relative sizes remain unchanged.

throughout the mathematical formalism of the analysis. This permits the analysis of shape variability both in a multivariate setting and in a morphological context. The visualization of the resulting patterns of shape variation is therefore of central importance to permit their interpretation in terms of underlying biological mechanisms. During visualization of shape variation with D'Arcy Thompson-style deformation grids, the correspondence between geometric and biological homology is no longer explicit, as reference is made to an external system of coordinates. Here we proposed a method to visualize shape change with direct reference to biological surface structures and showed that this technique facilitates the identification of differential patterns of development in cranial subunits.

Before we proceed to a more detailed characterization of these properties, we must consider a principal issue of GMM, namely the biological relevance of the geometric representation of organismic structures. In this study, we quantified shape variation with a relatively small set of landmarks ($p = 63$), which preserve their biological identity throughout the sample. On the one hand, the principal patterns of shape variation were subsequently visualized on the surface of the consensus cranium ($v = 3'310$ vertices), using TPS interpolation functions (equation (2.5)). This approach uses '*a posteriori*' interpolation to provide an easy visual grasp of the results. On the other hand, the '*a priori*' interpolation approach starts with an extended set of surface-bounded 'semi-landmarks' (Bookstein 1997), which are obtained through interpolation techniques relying on local geometrical properties of the object surface (Cutting *et al.* 1993, 1995; Bookstein 1997; Bookstein *et al.* 1999; Andresen *et al.* 2000). The resulting gain in sampling density, however, does not necessarily entail greater biological significance of the analysis, because semi-landmarks are placed according to geometric rather than biological homology criteria. While this latter approach is highly valuable for clinical predictive studies and the quantization of shape differences, the former may be preferred in studies aiming at the identification of growth processes underlying patterns of shape change and differences between shapes.

(b) *Symmetrization of specimens*

Two alternative methods were proposed to constrain the analysis to symmetrical modes of shape variation. Behind these methods are different basic assumptions about the causes and structure of asymmetric shape variation in the sample. On the one hand, sample-symmetrization presupposes a common cause of deviation from symmetry in all specimens, such that the sample consensus represents the best estimate of a symmetric reference. Self-symmetrization, on the other hand, does not presuppose a uniform mode of deviation from symmetry. This method is therefore most appropriate to eliminate asymmetry in a heterogeneous sample, which comprises, for example, fossil specimens exhibiting deviations from symmetry due to taphonomic deformation (Ponce de

León & Zollikofer 2001). Nevertheless, it appears that, in practical applications, the choice of methods hardly influences the outcome of the analyses.

(c) *Shape variation in human crania*

Figure 1*b* shows that the cranio-mandibular ontogeny follows a fairly linear trajectory through shape space (along PC1), implying that the spatial patterns of shape change (as visualized in figure 3*a*,*b*) remain constant between the age of 3 years and adulthood. A recent analysis combining GMM with histomorphologic data (O'Higgins & Jones 1998) showed that linear trajectories further imply a constant spatial distribution of depository and resorptive cranial growth fields. Figure 1*b* therefore, is in concordance with earlier direct observations (Enlow 1990), indicating that the growth fields of the human cranium are conserved from the age of 3 years to adulthood.

Figure 3 provides a visual representation of these results. We focus here on the patterns of shape change visible on the external surfaces of the craniomandibular morphology (a more detailed account including internal basicranial surfaces will be given elsewhere). Figure 3*a*,*b* reveals distinct developmental characteristics of the viscerocranial and neurocranial regions of the skull, most conspicuously expressed by their positive and negative allometric growth rates, respectively. The relative developmental autonomy of the viscerocranium and the neurocranium is a well-documented fact of cranial morphogenesis (Enlow 1990; Larsen 1993; Lieberman *et al.* 2000*b*). More specifically, the contrasting allometric growth rates of these developmental modules concur with the observation that the human brain expands rapidly during the first few years of postnatal life, such that neurocranial growth is virtually complete around the age of 3 years, while the subsequent phases of ontogeny are dominated by expansion of the masticatory system.

As indicated in figure 2, advancement along PC1 describes not only age-related but also size-related variation in shape. Accordingly, figure 3*a*,*b* represents not only developmental changes in shape but also size allometry among adults. It is instructive to compare these findings with classical allometric analyses showing a trend from brachycephaly to dolichocephaly with increasing size of the human skull (Huxley 1932). This trend corresponds to shape variation along PC1, i.e. from broad, short, more paedomorphic skulls to narrow, elongated, more peramorphic skulls.

Our analyses revealed that, independent of age and size, an important proportion of cranial shape variability (11%, as accounted for by PC2) can be traced back to differences in the position and orientation of the face and masticatory system relative to the braincase. It is interesting to note that this mode of shape variation describes size-independent transition between 'brachycephalic' and 'dolichocephalic' extreme shapes: as opposed to the reported size-related variation between such cranial shapes. This seeming incongruity points at an important issue of morphological terminology already recognized a century ago (Martin 1901), as it shows that classical morphological terms do not necessarily denote biologically meaningful entities. Brachycephaly versus dolichocephaly essentially describes the degree of cranial sphericity. The finding that two statistically independent modes of shape variation (PC1 and PC2) influence this visually salient feature of the human skull may by indicative of at least two distinct underlying morphogenetic processes. While one (PC1) is probably related to growth allometry, another (PC2) may be related to positional shifts of the viscerocranium relative to the neurocranium. Basing on evidence provided by Lieberman *et al.* (2000*a*,*b*), we propose that the latter mode of variation reflects early developmental variation in the basicranium: this region forms an embryonic supportive structure for the brain on one side and the face and masticatory system on the other (Larsen 1993; Lieberman *et al.* 2000*a*,*b*), such that it may constrain the morphogenesis of these adjacent structures and give rise to the observed postnatal pattern of correlated shape variation. In their analysis of basicranial influence on overall cranial shape, Lieberman *et al.* (2000*a*) specifically show that the degree of brachycephaly versus dolichocephaly depends on the interaction between cranial base width and endocranial size. Our study parallels these findings to some extent, indicating that changes in cranial base width (as visible in the ear region; see figure 3*b*,*c*) play an important role in the mode of cranial shape variation described by PC2.

Our pooled-population/pooled-sex sample was chosen with the intention to capture the basic *H. sapiens* pattern of postnatal cranio-mandibular development. As *H. neanderthalensis* followed essentially the same pattern of development (Ponce de León & Zollikofer 2001), it is probable that we observe here a shared ancestral mode of cranial ontogeny, possibly of the genus *Homo*. Further research is required in two directions: (i) to investigate the more subtle differences between population-specific and sex-specific temporal and spatial patterns of modern and fossil human cranial ontogeny; and (ii) to study, in more detail, developmental shape variation of both external and internal cranial structures, notably with respect to the developmental role of the cranial base in relation to the viscerocranium and neurocranium (Lieberman *et al.* 2000*a*). From a general perspective, the methods proposed here—self-symmetrization of bilateral landmark configurations and surface-based visualization of shape change—have been shown to be efficient tools for the analysis of the morphogenetic background of complex patterns of shape variability.

We dedicate this paper to the memory of Leslie Marcus. We are grateful to P. Stucki for constant support of our research and thank Gea Bijl for technical assistance during CT scanning of the cranial sample. We also thank the anonymous reviewers for their constructive comments on the manuscript. This work was supported by Swiss NSF grant no. 31-42419.94 and a habilitation grant of the Canton of Zurich.

REFERENCES

Adams, D. C. & Rohlf, F. J. 2000 Ecological character displacement in *Plethodon*: biomechanical differences found from a geometric morphometric study. *Proc. Natl Acad. Sci. USA* **97**, 4106–4111.

Andresen, P. R. & Nielsen, M. 2001 Non-rigid registration by geometry-constrained diffusion. *Med. Image Anal.* **5**, 81–88.

Andresen, P. R., Bookstein, F. L., Conradsen, K., Ersboll, B. K., Marsh, J. L. & Kreiborg, S. 2000 Surface-bounded growth modeling applied to human mandibles. *IEEE Trans. Med. Imaging* **19**, 1053–1063.

Auffray, J. C., Alibert, P., Renaud, S., Orth, A. & Bonhomme, F. 1996 Fluctuating asymmetry in *Mus musculus* subspecific hybridization: traditional and Procrustes comparative approach. In *Advances in morphometrics* (ed. L. F. Marcus, M. Corti, A. Loy, G. Naylor & D. E. Slice), pp. 275–283. New York: Plenum Press.

Bookstein, F. L. 1991 *Morphometric tools for landmark data*. Cambridge University Press.

Bookstein, F. L. 1997 Landmark methods for forms without landmarks: morphometrics of group differences in outline shape. *Med. Image Anal.* **1**, 225–243.

Bookstein, F. L. (and 12 others) 1999 Comparing frontal cranial profiles in archaic and modern *Homo* by morphometric analysis. *Anat. Rec.* **257**, 217–224.

Cutting, C. B., Bookstein, F. L., Haddad, B., Dean, D. & Kim, D. 1993 A spline-based approach for averaging three-dimensional curves and surfaces. *Proc. Soc. Photo-opt. Imaging Engng* **2035**, 29–44.

Cutting, C. B., Dean, D., Bookstein, F. L., Haddad, B., Khorramabadi, D., Zonneveld, F. W. & McCarthy, J. G. 1995 A three-dimensional smooth surface analysis of untreated Crouzon's syndrome in the adult. *J. Craniofac. Surg.* **6**, 444–453.

Dryden, I. L. & Mardia, K. 1998 *Statistical shape analysis*. New York: Wiley.

Emlen, J. M., Freeman, D. C. & Graham, J. H. 1993 Nonlinear growth dynamics and the origin of fluctuating asymmetry. *Genetica* **89**, 77–96.

Enlow, D. H. 1990 *Facial growth*. Philadelphia, PA: Saunders.

Huxley, J. 1932 *Problems of relative growth*. London: Methuen.

Klingenberg, C. P. & Nijhout, H. F. 1999 Genetics of fluctuating asymmetry: a developmental model of developmental instability. *Evolution* **53**, 358–375.

Klingenberg, C. P., McIntyre, G. S. & Zaklan, S. D. 1998 Left–right asymmetry of fly wings and the evolution of body axes. *Proc. R. Soc. Lond.* B **265**, 1255–1259.

Larsen, W. J. 1993 *Human embryology*. New York: Churchill Livingstone.

Lele, S. 1993 Euclidean distance matrix analysis (EDMA): estimation of mean form and mean form difference. *Math. Geol.* **25**, 573–602.

Lieberman, D. E., Pearson, O. M. & Mowbray, K. M. 2000*a* Basicranial influence on overall cranial shape. *J. Hum. Evol.* **38**, 291–315.

Lieberman, D. E., Ross, C. F. & Ravosa, M. J. 2000*b* The primate cranial base: ontogeny, function, and integration. *Yearbook Phys. Anthropol.* **43**, 117–169.

Loy, A., Corti, M. & Marcus, L. F. 1993 Landmark data: size and shape analysis in systematics. A case study on Old World Talpidae (Mammalia, Insectivora). In *Contributions to morphometrics* (ed. L. Marcus, E. Bello & A. García-Valdecasas), pp. 215–240. Madrid: Consejo superior de investigaciones científicas.

Lynch, J. M., Wood, C. G. & Luboga, S. A. 1996 Geometric morphometrics in primatology: craniofacial variation in *Homo sapiens* and *Pan troglodytes*. *Folia Primatol.* **67**, 15–39.

McCollum, M. A. 1999 The robust australopithecine face: a morphogenetic perspective. *Science* **284**, 301–305.

Mardia, K. V., Bookstein, F. L. & Moreton, I. J. 2000 Statistical assessment of bilateral symmetry of shapes. *Biometrika* **87**, 285–300.

Martin, R. 1901 *Anthropologie als Wissenschaft und Lehrfach. Eine akademische Antrittsrede*. Jena, Germany: Gustav Fischer.

Moss, M. L. & Young, R. W. 1960 A functional approach to craniology. *Am. J. Phys. Anthropol.* **18**, 281–292.

O'Higgins, P. 2000 The study of morphological variation in the hominid fossil record: biology, landmarks and geometry. *J. Anat.* **197**, 103–120.

O'Higgins, P. & Jones, N. 1998 Facial growth in *Cercocebus torquatus*: an application of three-dimensional geometric morphometric techniques to the study of morphological variation. *J. Anat.* **193**, 251–272.

Ponce de León, M. S. & Zollikofer, C. P. E. 2001 Neanderthal cranial ontogeny and its implications for late hominid diversity. *Nature* **412**, 534–538.

Rao, C. R. & Suryawanshi, S. 1998 Statistical analysis of shape through triangulation of landmarks: a study of sexual dimorphism in hominids. *Proc. Natl Acad. Sci. USA* **95**, 4121–4125.

Richtsmeier, J. T. & Lele, S. 1993 A coordinate-free approach to the analysis of growth patterns: models and theoretical considerations. *Biol. Rev.* **68**, 381–411.

Richtsmeier, J. T. & Walker, A. 1993 A morphometric study of facial growth. In *The Nariokotome* Homo erectus *skeleton* (ed. A. Walker & R. Leakey), pp. 391–410. Cambridge, MA: Harvard University Press.

Richtsmeier, J. T., Corner, B. D., Grausz, H. M., Cheverud, J. M. & Danahey, S. E. 1993 The role of postnatal growth pattern in the production of facial morphology. *Syst. Biol.* **42**, 307–330.

Rohlf, F. J. & Marcus, L. 1993 A revolution in morphometrics. *Trends Ecol. Evol.* **8**, 129–132.

Rohlf, F. J. & Slice, D. 1990 Extensions of the Procrustes method for the optimal superimposition of landmarks. *Syst. Zool.* **39**, 40–59.

Thompson, D. A. W. 1948 *On growth and form*. Cambridge University Press.

Ubelaker, D. H. 1978 *Human skeletal remains. Excavations, analysis, interpretation*. Chicago University Press.

Yaroch, L. A. 1996 Shape analysis using the thin-plate spline: Neanderthal cranial shape as an example. *Yearbook Phys. Anthropol.* **39**, 43–89.

Zelditch, M. L., Bookstein, F. L. & Lundrigan, B. L. 1992 Ontogeny of integrated skull growth in the cotton rat *Sigmodon fulviventer*. *Evolution* **45**, 1154–1180.

As this paper exceeds the maximum length normally permitted, the authors have agreed to contribute to production costs.

Visit http://www.pubs.royalsoc.ac.uk to see an electronic appendix to this paper.